RSC Advances

ROYAL SOCIETY OF CHEMISTRY

www.rsc.org/advances

Synthesis and Characterization of Biocompatible Gymnemic Acid-Gold Nanoparticles: A Study on Glucose Uptake Stimulatory Effect in 3T3-L1 Adipocytes

T. Rajarajeshwari, C. Shivashri, P. Rajasekar*

Department of Biotechnology, Rajalakshmi Engineering College, Thandalam, Chennai-602 105, Tamil Nadu
Email: rajarajeshwari.t@gmail.com, shivashri.cj@gmail.com

***Corresponding Author**
Dr. P. Rajasekar
Assistant Professor (SS)
Department of Biotechnology
Rajalakshmi Engineering College
Thandalam
Chennai-602 105
Tamil Nadu
India
Fax: +91 44 37181113
Email: rajasekar.panchamurthy@gmail.com

Abstract

The study biosynthesized gold nanoparticles using gymnemic acid (GA), a secondary metabolite of *Gymnema sylvestre*. The gymnemic acid reduced gold nanoparticles (GA-AuNPs) were primarily confirmed from the colour change and UV absorption. The reducing potential of GA was computed and free GA was quantified after the biosynthesis of GA-AuNPs using HPLC. The size, charge, shape, crystalline nature and functional groups of GA-AuNPs were studied by TEM, DLS, XRD and FT-IR analysis respectively. The stability of GA-AuNPs in various physiological buffers and pH was examined. The cytotoxicity of GA-AuNPs and the comparative glucose utilization effect of GA and GA-AuNPs were analysed. The GA-AuNPs appeared in ruby red colour and showed UV absorption at 540 nm. The reducing efficiency of GA was found to be 98%. The complete utilization of GA (100%) after the biosynthesis of GA-AuNPs was observed in the HPLC chromatogram. The GA-AuNPs displayed a spherical morphology under TEM analysis. The DLS analysis of GA-AuNPs revealed an average size of 62.93 nm and a zeta potential of -14 mV. The XRD data confirmed the nature of GA-AuNPs to be face centered cubic (fcc) crystals and its stability was identified from the FT-IR spectra. The GA-AuNPs showed a remarkable stability in the various medium and displayed 56.67% cell viability at 1000 µM concentration in 3T3-L1 adipocytes. The adipocytes treated with GA and GA-AuNPs displayed a minimal and a dose-dependent rise in glucose uptake respectively, demonstrating enhanced bioavailability mediated glucose utilization. The study suggests that GA-AuNPs might serve as an effective plant-based oral formulation for the treatment of hyperglycemia.

Keywords: Gymnemic acid, gold nanoparticles, morphology, stability, 3T3-L1 adipocytes, cytotoxicity, glucose uptake

Introduction

Nanomedicine is an emerging field that offers eco-friendly treatment with increased therapeutic efficiency by enhancing the bioavailability, reducing the toxicity and side effects of drugs. The bio-reduced gold and silver nanoparticles facilitate drug targeting to specific cells/tissues, indicating the potential role of gold nanoparticles in the field of medical biotechnology. It has been shown that gold nanoparticles are widely used in the treatment of various medical complications including diabetes.[1] Manikanth *et al.*[2] have proven the anti-diabetic potential of AuNPs in diabetic mice. It is also demonstrated that the phytochemical, guavanoic acid-reduced gold nanoparticles inhibits PTP-1B enzyme activity *in vitro,*[3] suggesting the modulating action of bioactive gold nanoparticles at the level of post-receptor signalling molecule.

Gymnema sylvestre is a medicinal plant commonly known as '*Gurmar*' in India. It is also called as 'sugar eater'. It has traditional medicinal values and used to treat asthma, cough, eye ailments, inflammations and snake bite. It shows various pharmacological properties and acts as anti-hypercholestremic, hepatoprotective and anti-saccharine agent.[4] It has been reported that the hypoglycemic action of *Gymnema sylvestre* is due to its bioactive components including gymnemic acid.[5]

Gymnemic acid (GA) is a mixture of pentacyclic triterpene glucuronides, widely used as a folk medicine for the treatment of metabolic disorders. It shows antioxidant, anti-saccharine and anti-inflammatory activities.[6,7] However, it has been shown that, the bioavailability of GA is poor due to its complex structure, lipid insolubility and membrane impermeability which eventually affects its entry into the systemic circulation.[8] This suggests that the beneficial impact of any herbal constituent(s) depend upon its absorption and bioavailability. Thus, the study hypothesized that the gymnemic acid-reduced gold nanoparticles (GA-AuNPs) would be an effective and suitable formulation to overcome the

structural complexity linked with the poor absorption and reduced bioavailability of plain GA. In addition, the nanonized GA-AuNPs would also be a simple form of oral drug in the treatment of diabetes. Therefore, the present study synthesized GA-AuNPs and performed its characterization by physical observation and spectral studies. The bio-reducing efficiency of GA was computed and confirmed from its HPLC quantification after the synthesis of GA-AuNPs. The size, shape, charge and nature of the synthesized GA-AuNPs were examined by TEM, DLS and XRD analysis. The functional groups responsible for the structural stability of GA-AuNPs were studied by FT-IR analysis. The stability of GA-AuNPs was examined in various physiological medium and in buffer solutions. The cytotoxicity and glucose utilization of GA-AuNPs were also evaluated in the differentiated 3T3-L1 adipocytes.

Experimental

Materials

Chloroauric acid ($HAuCl_4$), 6-(N-(7-nitrobenz-2-oxa-1,3-diazol-4-yl)amino)-2-deoxyglucose (6-NBDG), Insulin, Pioglitazone, L-glutamine and 3-(4,5-Dimethylthiazol-2-yl)-2,5-Diphenyltetrazolium Bromide (MTT) were of 99.9% purity, purchased from Sigma Aldrich, St Louis, MO, USA. High Glucose - Dulbecco's Modified Eagle's Medium (HG-DMEM) medium and calf serum (99% purity) was purchased from Gibco BRL, Grand Island, NY. Gymnemic acid (99%) was a kind gift from SV Agrofood, Navi Mumbai, India. All other chemicals and reagents were of analytical grade with 99% purity and purchased from Hi-Media Laboratories Pvt. Ltd.

Methods

Biosynthesis of gold nanoparticles using gymnemic acid

Chloroauric acid (1 mM) was prepared in deionized water. The solution was heated at 80°C and cooled at room temperature (37°C). GA (30 mg) was dissolved in 1 mL of distilled water and mixed with 49 mL of $HAuCl_4$ solution. The mixture was then sonicated at 40 kHz and 135 W for 30 min using an ultra-sonication homogenizer (Omni Rupter 250, Omni International Inc.) in order to prevent agglomeration and to obtain uniform nanoparticles.[9] The mixture was placed in an orbital shaker for 1 h at 37°C for the complete reduction of gold ions by GA. The GA-AuNPs suspension was centrifuged using a cooling centrifuge at 6000 rpm for 15 min. The supernatant was collected and the λ max was recorded using the UV-Vis Spectrophotometer (Lamda 35, Perkin Elmer) and the same was used for characterization and stability analysis.

Bio-reduction efficiency of gymnemic acid

The bio-reduction efficiency of GA was estimated by the method of Mukhopadhyay *et al*.[10] with slight modifications. Briefly, a standard graph was plotted at 230 nm,[11] which is the maximum absorption range of pure GA. The concentration of the unreacted GA present in the suspension of GA-AuNPs was estimated at 230 nm and compared with the standard graph of pure GA. The bio-reduction efficiency of GA was calculated by

$$\text{Bio-reduction efficiency (\%)} = \frac{\text{Initial concentration of GA} - \text{Concentration of unreacted GA}}{\text{Initial concentration of GA}} \times 100$$

HPLC Analysis

The free GA content in the biosynthesized gold nanoparticle suspension was quantified using a water HPLC system (Shimadzu, Model SPD-20A, Japan) [injection volume 20 µL, two 510 pumps, 7725 Rheodyne auto injector, a DUG-12 A degasser, SCL-10Avp system controller, C18 (ODS) reversed phase column (150 mm × 4.6 mm i.d., 5 µm particle size) and water 486 UV detector (all from Shimadzu, Kyoto, Japan)]. The

mobile phase consisted of 0.1% acetic acid; water/methanol (v/v) (35:65, HPLC grade) delivered at a constant flow rate of 1 mL min^{-1}. The chromatogram of GA-AuNPs was compared with the chromatogram of standard GA. All the determinations were carried out in duplicates.

Transmission Electron Microscopic Analysis (TEM)

Samples for TEM analysis were prepared by placing a drop of the gold colloidal solution on a TEM copper grid (200 meshes; carbon-coated). The film on the copper grid was dried and the excess solution was removed using blotting paper. TEM measurements were performed on TECNAI 10 Philips; the instrument was operated at an accelerating voltage of 100 KV. The size and shape of the bio-reduced gold nanoparticles were obtained from the TEM images.

Dynamic Light Scattering (DLS) Analysis

The size and zeta potential of GA-AuNPs was measured by DLS with a Zetasizer Ver. 7.03 (Malvern Instrument, UK) at 25°C to investigate its aggregation tendency and stability after 48 h. To avoid the influence of dust on the reliability of results, the solutions of GA-AuNPs was filtered through a 0.5 µm millipore filter before testing.

X-Ray Diffraction analysis (XRD)

The lyophilised powder of GA-AuNPs was placed onto a glass substrate and analysed using a powder X-ray diffractometer (XDL 3000, X'pert PRO-MPD) operated at a voltage of 30 kV and a current of 100 mA with Cu Kβ filter.

Fourier Transform Infrared Analysis (FT-IR)

Fourier Transform Infrared (FT-IR) analysis was carried out in KBr matrix using JASCO 460 plus spectrophotometer with a frequency ranging from 4000-400 cm^{-1}. The baseline corrections were performed for all spectra.

***In vitro* stability analysis**

The *in vitro* stability of GA-AuNPs was examined in various physiological medium (10% NaCl, 0.5% BSA, 0.2 M Histidine and 0.2 M Cysteine) and in phosphate buffer solutions pertaining to acidic (1.2 & 5), and alkaline (7.4 & 9) pH. Briefly, 0.5 mL of GA-AuNPs suspension was mixed with 0.5 mL each of the physiological medium and buffer solutions and its maximum absorbance was recorded after 24 h using the UV-Vis Spectrophotometer.

Cell culture

3T3-L1 pre-adipocytes were purchased from National Centre for Cell Sciences (NCCS), Pune with a Passage No. 36. The pre-adipocytes were maintained in HG-DMEM [supplemented with 10% calf serum, 2 mM L-glutamine, penicillin (100 units mL^{-1}) and streptomycin (100 μg mL^{-1})] and incubated at 5% CO_2 and 37°C for 24 h in a CO_2 incubator. For the differentiation of pre-adipocytes, cells were incubated in DMEM [supplemented with 10% FBS, insulin (5 mg mL^{-1}), dexamethasone (250 nM) and isobutylmethylxanthine (500 mM)] for 5 days and the well differentiated adipocytes were observed as multinucleated cells.

Cytotoxicity Assay

The cytotoxicity was assessed by MTT. The assay is based on the conversion of MTT to formazon crystals by living cells, which determines mitochondrial activity. Briefly, the adipocytes (5×10^4 cells per well) were plated in 96-well plate and incubated for 24 h. The medium was then replaced with 100 µL of fresh medium containing different concentrations of GA-AuNPs (1, 3, 10, 30, 100, 300 and 1000 µM per well). Untreated cells served as control. At the end of the treatment period, media from the control and drug treated cells was discarded and 50 µL of MTT (5 mg mL^{-1} PBS) was added and incubated for 4 h at 37°C in a CO_2 incubator. The MTT was discarded and the cells were then solubilized in 200 µL of DMSO. The coloured, solubilized formazon dye was measured using an ELISA reader (Model 680, Biorad) at 570 nm.

Glucose uptake Assay in 3T3-L1 Adipocytes

The glucose uptake assay was performed by the method of Yonemitzu *et al.*[12] with minor modifications. Briefly, the differentiated 3T3-L1 adipocyte cells (5×10^4 cells per well) were starved in serum-free HG-DMEM for 2 h and incubated with 200 µL of the differentiation medium containing plain GA (30 µg per well), various concentrations of GA-AuNPs (1, 3 10, 30 µg per well), standard drug (pioglitazone 10 µM) and human insulin (10 µM) for 24 h. Then, the pioglitazone, GA and GA-AuNPs treated cells were stimulated with 10 µM of insulin for 15 min. Later, the medium was discarded and cells were incubated with 100 µL of 20 µM 6-NBDG for 30 min. The cells were then washed with DPBS (Dulbecco`s Phosphate Buffered Saline) and lysed with 70 µL of lysis buffer for 10 min at dark. The lysed cells were mixed with 30 µL of DMSO and the fluorescence was measured using a microplate reader with an excitation/emission wavelength of 466/540 nm.

Statistical Analysis

Values are expressed as means ± SD. Data within the groups are analysed using one way analysis of variance (ANOVA) followed by Duncan's Multiple Range Test (DMRT). Value of $p<0.05$ was considered statistically significant. All *in vitro* experiments were carried out in triplicates (n=3).

Results

Colour change and UV absorption spectrum of GA-AuNPs

Fig. 1 shows the original colour of $HAuCl_4$ solution (pale yellow) (a). The initial colour of $HAuCl_4$ was changed to bright ruby red colour after 30 min of GA reaction (b). The

UV-Vis absorption of GA-AuNPs was recorded after 1 h and 48 h of GA reaction with $HAuCl_4$ (Fig. 2). The GA-AuNP showed a distinct surface plasmon resonance at 540 nm after 1 h. However, the extent of UV absorption increased steadily after 48 h and showed λ max at the same wavelength. The observed characteristic colour transformation and the range of UV absorption confirmed the GA mediated bio-reduction of $HAuCl_4$.

Bio-reduction efficiency of gymnemic acid

The bio-reduction efficiency of GA for the synthesis of GA-AuNPs was computed and the concentration of GA involved during the reaction was found to be 98%.

HPLC Chromatogram of GA and GA-AuNPS

Fig. 3 shows the HPLC chromatogram of pure GA (a) and GA-AuNPs (b). In order to confirm the computed bio-reducing potential of GA, the study performed HPLC quantification of free GA [i.e the remaining GA after the bio-reduction of $HAuCl_4$] in the biosynthesized gold nanoparticles and compared with pure GA as standard. In the HPLC chromatogram, pure GA produced a sharp peak with retention time 2.500 min. However, the GA treated gold solution did not produce any peak for free GA when compared with the pure standard, demonstrating the complete (100%) entrapment of GA on gold surface during the biogenesis of GA-AuNPs.

TEM images of GA-AuNPs

Fig. 4 shows the TEM images of GA-AuNPs, revealing the morphology and size of the nanoparticles. The TEM micrographs of GA-AuNPs showed the size of the NPs ranging from 22-55 nm and the particles were found to be predominantly spherical in shape.

Particle size and zeta potential of GA-AuNPs

Figure 5 shows the average size (a) and zeta potential (b) of GA-AuNPs. The average size and zeta potential of GA-AuNPs were obtained by DLS analysis. The graph representing the size of GA-AuNPs displayed two peaks: peak 1 between 20–100 nm and peak 2 between 150–1000 nm, demonstrating the varied sizes of GA-AuNPs. However, the intensity of peak 1 was significantly greater than peak 2 indicating the average size of GA-AuNPs to be 62.93 nm. The zeta potential of GA-AuNPs was found to be -14.9 mV. The negative values of the nanoparticles demonstrate its stability.

XRD spectrum of GA-AuNPs

Fig. 6 gives the XRD spectrum of GA-AuNPs. In order to confirm the mono crystalline nature of gold NPs, the XRD analysis was performed. The XRD spectrum showed an intense, sharp characteristic peak for gold (111) appearing at $2\Theta = 38.49°$, indicating the structure of GA-AuNPs as face-centered cubic (fcc) crystals.

FT-IR spectrum of GA-AuNPs

Fig. 7 shows the FT-IR spectrum of plain GA (a) and its NPs (b). The FT-IR spectrum of GA-AuNPs was compared with the spectrum of pure GA for the elucidation of functional groups responsible for its stability. The spectrum of plain GA showed the peaks at 3412 cm^{-1} (O-H stretching), 2929 cm^{-1} (C-H stretching), 1707 cm^{-1} (C=O stretching), 1644 cm^{-1} (C=C stretching), 1538 cm^{-1} (C=C aromatic stretching) 1460 cm^{-1} (CH_2 bending), 1382 cm^{-1} (C-H bending) 1269 cm^{-1} and 1041 cm^{-1} (C-O stretching), 909 cm^{-1} (O-H bending) and 609 cm^{-1} (=C-H bending). This reveals that these atoms/groups of GA are exposed on its surface. On comparing the FT-IR spectrum of GA-AuNPs with pure GA, three peaks were shifted to lower frequencies (3398 cm^{-1}, 1635 cm^{-1}, and 1514 cm^{-1}) and four peaks were shifted to higher frequencies (2935 cm^{-1}, 1273 cm^{-1} 1078 cm^{-1} & 655 cm^{-1}). The peaks for C=O stretching (1707 cm^{-1}), CH_2 bending (1460 cm^{-1}) and O-H bending (909 cm^{-1})

disappeared in the spectrum of GA-AuNPs. This suggests the effective reduction of Au^{3+} to Au^{0} by carbonyl, primary alcoholic group and hydroxyl group of GA.

Stability of GA-AuNPs

Fig. 8 shows the stability of GA-AuNPs in different physiological medium (a) and in phosphate buffer solutions (b). The stability of GA-AuNPs is one of the important criteria for drug delivery and targeting. Thus, the stability of GA-AuNPs in various physiological medium (10% NaCl, 0.5% BSA, 0.2 M Histidine and 0.2 M Cysteine) and in phosphate buffer of different pH (1.2, 5, 7.4 & 9) was examined *in vitro*. The GA-AuNPs showed maximum absorption in the various physiological medium and in buffer solutions between the range 534-537 nm and 529-535 nm respectively. In both the medium, GA-AuNPs showed approximately 3 to 11 nm shift in their surface plasmon resonance, demonstrating a remarkable stability of the GA-AuNPs.

***In vitro* cytotoxicity of GA-AuNPs**

Fig. 9 shows the cytotoxic effect of GA-AuNPs in 3T3-L1 adipocytes. The cultured 3T3-L1 cells were exposed to various concentrations of GA-AuNPs [1, 3, 10, 30, 100, 300 and 1000 µM] and the percentage of viable cells were measured by MTT assay. The cellular toxicity of GA-AuNPs in 3T3-L1 adipocytes was identified at higher concentrations. The GA-AuNPs showed 56.67% cell viability at 1000 µM concentration.

***In vitro* glucose uptake efficiency of GA-AuNPs**

Fig. 10 depicts the glucose uptake efficiency of GA and GA-AuNPs in 3T3-L1 adipocytes. The effect of GA and GA-AuNPs on glucose uptake was monitored by 6-NBDG assay. The 3T3-L1 adipocytes were pre-incubated with plain GA (30 µg) and different concentrations [1µg, 3 µg, 10 µg and 30 µg] of GA-AuNPs, insulin (10 µM) and pioglitazone

(10 µM) for 24 h. The plain GA incubated 3T3-L1 adipocytes displayed a glucose uptake of 25.27% when compared with insulin (32.89%) and pioglitazone (52.76%) respectively. However, the effect of GA-AuNPs on glucose utilization in 3T3-L1 adipocytes was more pronounced (i.e) a dose-dependent increase in glucose uptake was noted in the GA-AuNPs treated adipocytes. The adipocytes treated with 30 µg GA-AuNPs displayed maximum (49.43%) uptake of 6-NBDG, when compared with plain GA, confirming its bioavailability associated synergetic/additive action. The observed effect of GA-AuNPs on glucose utilization was similar to the effect of pioglitazone (52.76%).

Discussion

The study biosynthesized and characterized gymnemic acid reduced gold nanoparticles (GA-AuNPs) and evaluated its efficiency on glucose utilization in the cultured 3T3-L1 adipocytes, for the development of potent nano-based anti-diabetic drug. The effective bio-reduction of Au^{3+} to Au^{0} by GA signifies the interaction of unpaired pi-electrons/exposed active functional group(s) of GA with Au^{3+} and thereby generate stable GA impregnated AuNPs. It has been believed that the colour transformation and the range of UV absorption for bio-reduced metallic nanoparticles are important characteristic features for its preliminary confirmation.[13] In the present study, the formation of GA reduced AuNPs are evident by its colour change from pale yellow to bright ruby red colour.[14] The range of UV absorption for gold nanoparticles are well documented,[15,16] which is similar to the UV absorption of GA-AuNPs, demonstrating the effective bio-reduction of $HAuCl_4$ by GA. The effective bio-reducing efficiency of GA is further confirmed from its computed bio-reduction efficiency (98%) and a complete disappearance of peak for GA (100% utilization) in the HPLC chromatogram of GA-AuNPs. The colour transformation and UV absorption of GA-AuNPs are mainly due to the surface plasmon resonance, mediated by

the collective oscillation of free electrons in the conduction band of nanoparticles induced by the interacting electromagnetic field.[17]

The green synthesis of noble metal nanoparticles using plant or fruit extracts has been well established to form crystalline nanoparticles in various shapes and sizes ranging from 1-100 nm.[17] The TEM micrographs of GA-AuNPs proved its shape as spherical with sizes < 55 nm. Our results were corroborated with the finding of Kalpana *et al.*[18] who have observed the spherical morphology with sizes < 80 nm for the plant powder reduced gold nanoparticles. The size and shape of nanoparticles are mostly determined by various factors such as the nature of plant extract and its concentration, metal salt, pH, temperature, extent of reaction time and the mixing ratio of plant extract and metal salt.[19]

The DLS analysis of GA-AuNPs provides the average size of nanoparticle (62.93 nm) and the zeta potential (-14 mV). The disparity in the size of GA-AuNPs under TEM and DLS analysis is presumably due to the nature of nanoparticles used during the examination. For example, a dried nanoparticle sample on grid is used for TEM analysis, whereas the DLS analysis is performed in direct hydrodynamic volume.[20] The difference in the nature of sample processing might possibly influence the variation in the size of GA-AuNPs. The zeta potential is a parameter widely used to predict colloidal suspension stability. It provides the degree of repulsion between similarly charged particles in dispersion medium. It has been well established that the stability of NPs depends upon its charge. The greater stability of nanoparticles is associated with its negative charge (i.e) nanoparticles with more negative charge (< -30) showed a greater stability.[21] The observed stability of GA-AuNPs might be associated with its measured negative charge (i.e) the zeta potential of GA-AuNPs.

The physical nature (i.e. crystalline nature) of GA-AuNPs was obtained from its XRD spectrum. The persistence of an intense peak at $2\Theta = 38.49°$ corresponds to (111), confirming

that the GA-AuNPs are face centered cubic crystals (JCPDS, file no. 04-0784) and lying flat on the planar surface.[22]

The possible functional group(s) of GA responsible for the bio-reduction of Au^{3+} and its stabilization were established through the FT-IR analysis. On comparing the FT-IR spectrum of plain GA-AuNPs with GA, the peak shifts to lower frequencies (3398 cm^{-1}, 1635 cm^{-1}, and 1514 cm^{-1}) indicate the O-H stretching, C=C stretching and C=C aromatic stretching respectively. Similarly, the peak shifts to higher frequencies illustrate the C-H stretching (2935 cm^{-1}), C-O stretching (1273 cm^{-1} & 1078 cm^{-1}) and =C-H bending (655 cm^{-1}). Also the disappearance of the peak for C-O stretching (1707 cm^{-1}), bending of CH_2 (1460 cm^{-1}) and O-H bending (909 cm^{-1}) indicate the effective participation of these groups during the reduction of Au^{3+} to Au^0 without any structural modification. The complete utilization (100%) of GA after the biosynthesis of GA-AuNPs is also confirmed from its HPLC chromatogram. It has been documented that the bio-organic compounds like flavones, polyphenols, terpenoids, monosaccharide like glucose, polysaccharides etc. can reduce metal ions efficiently without changing the structure.[23,14] The reducing sugar in the medium can reduce metal ions and form corresponding metal nanoparticles. It is also possible that the oxidized aldehyde group of sugar (i.e COOH group) can interact on metal surface.[23] The amino acid tyrosine reduces gold and silver ions and thereby forming Au and AgNPs. It has been documented that the semiquinone, amine and carboxylic acid (must exist in ionic form: (i.e) COO^- carboxylate ion) groups of tyrosine are available to bind on the metallic surface; when working with pH higher than the pI of tyrosine.[24,25] It is also reported that during the reduction process the carboxylic group present in the plant extract becomes COO^- and act as surfactants for the attachment on the surface of gold.[26] From the FT-IR data of GA-AuNPs, it can be strongly concluded that during the biogenesis of GA-AuNPs, the $–COO^-$, O-H and primary alcoholic groups of the glycan

portion of GA might possibly interact with the gold surface through a strong electrostatic interaction without any structural modifications.

The stability of AuNPs in various physiological medium (NaCl, BSA, Histidine and Cysteine) and in wide range of physiological pH is important for biomedical applications, including drug targeting. The stability of GA-AuNPs in the different physiological solutions and in different pH suggests the possibility for the development of stable nano-based GA formulation for targeted action(s).

The bio-reduced AuNPs with varying sizes (1-500 nm) and shapes have been used for the various therapeutic applications.[27,28] The cytotoxic effect of nanoparticles is well documented and depends upon its size [size dependent cytotoxic effect is due to the the presence of coated surface ligands] and large surface to volume ratio.[29,30,31] The cytotoxic effect of gold complexes Au (I) and Au (III) are also well established.[32,33] The present study has proved the non-cytotoxic nature of GA-AuNPs at their lower doses.

The study compared the glucose uptake efficiency of GA and GA-AuNPs in 3T3-L1 adipocytes. It has been observed that, the adipocyte expression of GLUT4 gene is reduced in obese and glucose intolerant/diabetic subjects whereas, its expression is not altered in muscle cells.[34] Thus, the adipocytes are used as a model system to evaluate the glucose uptake and insulin resistant studies.[35]

It is well known that muscle cells and adipocytes utilize glucose predominantly by the translocation of GLUT4 transporters from the cytosol to the plasma membrane. The exocytosis of GLUT4 to the cell surface occurs through the insulin regulated pathway, involving the insulin receptor tyrosine kinase activity followed by the tyrosine phosphorylation of the insulin receptor substrate (IRS) proteins and the activation of a complex network of downstream molecules.[36,37] It is also possible that for the

insulin-independent glucose uptake, the translocation of GLUT4 to the plasma membrane is mediated by the activation of AMPK.[38]

Several reports have shown that AMPK and its signalling pathway is a potential molecular target in the development of drugs for the treatment of type 2 diabetes and obesity.[39,40,41] It is also believed that the naturally derived compounds such as berberine and S-allyl cysteine ameliorate diabetes and obesity by stimulating the activity of AMPK.[42,43] However, there are no detailed reports regarding the mechanism(s) of its activation. A recent study has demonstrated that, the cinnamon extract enhances glucose uptake in 3T3-L1 adipocytes by inducing GLUT4 translocation via AMPK stimulation through LKB1, a tumour suppressor protein expressed in all mammalian cells. It is observed that LKB1 has the tendency to phosphorylate and activate AMPK in response to metformin and energy depletion in cell lines.[44] It is also believed that the anti-diabetic action of plant derived quercetin and its glycosides is due to its inhibiting effect on mitochondrial ATP synthase, leading to the activation of AMPK.[45] The activation of AMPK by berberine is due to the increasing ratio of AMP/ATP, triggered by the inhibition of mitochondrial ATP biosynthesis.[46] This suggests that natural compounds/anti-diabetic agents have the tendency to phosphorylate and activate AMPK.

It is also documented that, GA exhibited a strong interaction with PTP-1B (Protein Tyrosine Phosphate-1B) in an *in silico* study.[47] The PTP-1B is a group of intracellular enzyme and recently proved to be a key regulator of insulin receptor activity and downstream signalling pathway. The lack of PTP-1B activates IRS, improves sensitivity to insulin, stimulates glucose uptake and also activates AMPK in the muscle and adipose tissue of mice.[48,49] GA also stimulates glucose uptake and promotes peripheral insulin sensitivity in experimentally induced diabetic animals.[50,51] It has been illustrated that the NPs with size < 100 nm can enter the cells and modulate the function(s).[52] The gold NPs (Size 72.8 nm) of

Gymnema sylvestre displays anti-cancer activity in human HT29 and Vero cell lines, demonstrating the membrane permeable nature of the nanoparticles.[53] In addition, guavanoic acid reduced gold NPs inhibits PTP-1B activity *in vitro*, explaining the interacting/modulating ability of NPs with post receptor molecules.[3]

In the present study, the short term stimulation of 3T3-L1 adipocytes by insulin following the treatment of plain GA displayed a minimal glucose uptake when compared with the effect of insulin. However, the GA-AuNPs treated adipocytes showed a concentration dependent enhancement in the glucose uptake efficiency when compared to plain GA and positive control, demonstrating enhanced bioavailability mediated additive/synergetic effect of GA-AuNPs with insulin. The findings lead us to hypothesize that the localized/entered GA-AuNPs might act as either a suppressor of mitochondrial ATP synthase/PTP-1B in the presence of insulin or an inducer of AMPK and its pre-signalling molecule, LKB1 in the absence of insulin. The eventual modulating action of GA-AuNPs could presumably enhance the glucose uptake efficiency of 3T3-L1 adipocytes by translocating the GLUT4 vesicle from the cytosol to the plasma membrane [Scheme I].

Conclusion

In conclusion, the results of the present study demonstrated that, GA-AuNPs enhanced the glucose utilization/uptake efficiency of 3T3-L1 adipocytes through the suggested insulin dependent/independent pathway and this bio-functionalized GA-AuNPs may be a potent glucose lowering agent in the management of diabetes. Our future studies *in vivo* will light on the exact mechanism(s) of action of GA-AuNPs on the disposal of glucose.

References

1. V. G. Kumar, S. D. Gokavarapu, A. Rajeswari, T. S. Dhas, V. Karthick, Z. Kapadia, T. Shrestha, I. A. Barathy, A. Roy, and S. Sinha, *Colloids Surf. B. Biointerfaces*, 2011, **87**, 159–63.

2. S. Barathmanikanth, K. Kalishwaralal, M. Sriram, S. R. K. Pandian, H. S. Youn, S. Eom, and S. Gurunathan, *J. Nanobiotechnology*, 2010, **8**, 16.

3. S. Khaleel Basha, K. Govindaraju, R. Manikandan, J. S. Ahn, E. Y. Bae, and G. Singaravelu, *Colloids Surf. B. Biointerfaces*, 2010, **75**, 405–9.

4. N. Komalavalli and M. V Rao, *Plant Cell. Tissue Organ Cult.*, 2000, **61**, 97–105.

5. G. S. Thakur, R. Sharma, B. S. Sanodiya, M. Pandey, G. Prasad, and P. S. Bisen, *J. Appl. Pharm. Sci.*, 2012, **2**, 1–6.

6. R. Galletto, V. L. D. Siqueira, E. B. Ferreira, A. J. B. Oliveira, and R. B. Bazotte, *Brazilian Arch. Biol. Technol.*, 2004, **47**, 545–551.

7. B. Ch, K. Rao, S. Gandi, and A. Giri, *World J. Microbiol. Biotechnol.*, 2012, **28**, 741–7.

8. R. A. Pathan, U. Bhandari, S. Javed, and T. C. Nag, *Indian J. Exp. Biol.*, 2012, **50**, 117–27.

9. J. H. Lee, S. U. S. Choi, S. P. Jang, and S. Y. Lee, *Nanoscale Res. Lett.*, 2012, **7**, 420.

10. P. Mukhopadhyay, K. Sarkar, M. Chakraborty, S. Bhattacharya, R. Mishra, and P. P. Kundu, *Mater. Sci. Eng. C*, 2013, **33**, 376–382.

11. A. B. A. Ahmed, a S. Rao, and M. V Rao, *Phytomedicine*, 2010, **17**, 1033–9.

12. S. Yonemitsu, H. Nishimura, M. Shintani, R. Inoue, Y. Yamamoto, H. Masuzaki, Y. Ogawa, K. Hosoda, G. Inoue, T. Hayashi, and K. Nakao, *Diabetes*, 2001, **50**, 1093–1101.

13. P. Daisy and K. Saipriya, *Int. J. Nanomedicine*, 2012, **7**, 1189–202.

14. D. MubarakAli, N. Thajuddin, K. Jeganathan, and M. Gunasekaran, *Colloids Surf. B. Biointerfaces*, 2011, **85**, 360–5.

15. T. H. Meen, J. K. Tsai, S. M. Chao, Y. C. Lin, T. C. Wu, T. Y. Chang, L. W. Ji, W. Water, W. R. Chen, I. T. Tang, and C. J. Huang, *Nanoscale Res. Lett.*, 2013, **8**, 450.

16. S. S. Lal. P.L.Nayak, *Int. J. Sci. Innov. Discov.*, 2012, **2**, 325–350.

17. S. Aswathy Aromal and D. Philip, *Spectrochim. Acta. A. Mol. Biomol. Spectrosc.*, 2012, **97**, 1–5.

18. D. Kalpana, P. B. T. Pichiah, A. Sankarganesh, W. S. Park, S. M. Lee, R. Wahab, Y. S. Cha, and Y. S. Lee, *J. Pharm. Innov.*, 2013, **8**, 265–275.

19. M. Noruzi, D. Zare, K. Khoshnevisan, and D. Davoodi, *Spectrochim. Acta. A. Mol. Biomol. Spectrosc.*, 2011, **79**, 1461–5.

20. G. Sharma, A. R. Sharma, R. Bhavesh, J. Park, B. Ganbold, J. S. Nam, and S. S. Lee, *Molecules*, 2014, **19**, 2761–70.

21. A. C. Puhl, M. Fagundes, K. Cristina, I. Polikarpov, M. Fátima, F. Silva, J. B. Fernandes, P. C. Vieira, M. R. Forim, and S. Carlos, 2011, **3**, 683–698.

22. P. K. Kar, S. Murmu, S. Saha, V. Tandon, and K. Acharya, *PLoS One*, 2014, **9**, e84693.

23. V. V Makarov, A. J. Love, O. V Sinitsyna, S. S. Makarova, I. V Yaminsky, M. E. Taliansky, and N. O. Kalinina, *Acta Naturae*, 2014, **6**, 35–44.

24. P. R. Selvakannan, A. Swami, D. Srisathiyanarayanan, P. S. Shirude, R. Pasricha, A. B. Mandale, and M. Sastry, *Langmuir*, 2004, **20**, 7825–7836.

25. P. Selvakannan, R. Ramanathan, B. J. Plowman, Y. M. Sabri, H. K. Daima, A. P. O'Mullane, V. Bansal, and S. K. Bhargava, *Phys. Chem. Chem. Phys.*, 2013, **15**, 12920–9.

26. P. K. Singh and S. Kundu, *J. Environ. Nanotechnol.*, 2013, **2**, 50–52.

27. H. Y. Wu, M. Liu, and M. H. Huang, *J. Phys. Chem. B*, 2006, **110**, 19291–4.

28. P. Ghosh, G. Han, M. De, C. K. Kim, and V. M. Rotello, *Adv. Drug Deliv. Rev.*, 2008, **60**, 1307–15.

29. T. Jennings and G. Strouse, in *Bio-Applications of Nanoparticles*, ed. Warren C.W. Chan, Landes Bioscience and Springer Science+Business Media, Tallahassee, 2007, pp. 34–47.

30. B. D. Chithrani, A. A. Ghazani, and W. C. W. Chan, *Nano Lett.*, 2006, **6**, 662–8.

31. J. A. Khan, B. Pillai, T. K. Das, Y. Singh, and S. Maiti, *Chembiochem*, 2007, **8**, 1237–40.

32. G. Oberdörster, E. Oberdörster, and J. Oberdörster, *Environ. Health Perspect.*, 2005, **113**, 823–839.

33. W. S. Cho, M. Cho, J. Jeong, M. Choi, H. Y. Cho, B. S. Han, S. H. Kim, H. O. Kim, Y. T. Lim, B. H. Chung, and J. Jeong, *Toxicol. Appl. Pharmacol.*, 2009, **236**, 16–24.

34. H. Ducluzeau, M. Fletcher, H. Vidal, M. Laville, and M. Tavar, *Diabetes Metab.*, 2002, **28**, 85–92.

35. M. J. Thomson, M. G. Williams, and S. C. Frost, *J. Biol. Chem.*, 1997, **272**, 7759–7764.

36. A. Virkamäki, K. Ueki, and C. R. Kahn, *J. Clin. Invest.*, 1999, **103**, 931–43.

37. A. H. Khan and J. E. Pessin, *Diabetologia*, 2002, **45**, 1475–83.

38. L. J. Goodyear and B. B. Kahn, *Annu. Rev. Med.*, 1998, **49**, 235–261.

39. K. A. Kenner, E. Anyanwu, J. M. Olefsky, and J. Kusari, *J. Biol. Chem.* , 1996, **271** , 19810–19816.

40. R. J. Gum, L. L. Gaede, S. L. Koterski, M. Heindel, J. E. Clampit, B. A. Zinker, J. M. Trevillyan, R. G. Ulrich, M. R. Jirousek, and C. M. Rondinone, *Diabetes* , 2003, **52** , 21–28.

41. A. J. Nichols, R. D. Mashal, and B. Balkan, *Drug Dev. Res.*, 2006, **67**, 559–566.

42. Y. S. Lee, W. S. Kim, K. H. Kim, M. J. Yoon, H. J. Cho, Y. Shen, J. M. Ye, C. H. Lee, W. K. Oh, C. T. Kim, C. Hohnen-Behrens, A. Gosby, E. W. Kraegen, D. E. James, and J. B. Kim, *Diabetes*, 2006, **55**, 2256–64.

43. Y. P. Hwang, H. G. Kim, J. H. Choi, M. T. Do, Y. C. Chung, T. C. Jeong, and H. G. Jeong, *J. Nutr. Biochem.*, 2013, **24**, 1469–1478.

44. R. J. Shaw, M. Kosmatka, N. Bardeesy, R. L. Hurley, L. A. Witters, R. A. DePinho, and L. C. Cantley, *Proc. Natl. Acad. Sci. United States Am.* , 2004, **101** , 3329–3335.

45. H. M. Eid, L. C. Martineau, A. Saleem, A. Muhammad, D. Vallerand, A. Benhaddou-Andaloussi, L. Nistor, A. Afshar, J. T. Arnason, and P. S. Haddad, *Mol. Nutr. Food Res.*, 2010, **54**, 991–1003.

46. M. Zhang and L. Chen, *Acta Pharm. Sin. B*, 2012, **2**, 379–386.

47. B. D. Bhagyashree Kamble, Ankur Gupta, Dada patil, *Am. J. pharmtech Res.*, 2012, **2**, 434–451.

48. H. G. Cheon, S. M. Kim, S. D. Yang, J. Du Ha, and J. K. Choi, *Eur. J. Pharmacol.*, 2004, **485**, 333–339.

49. B. Xue, T. Pulinilkunnil, I. Murano, K. K. Bence, H. He, Y. Minokoshi, K. Asakura, A. Lee, F. Haj, N. Furukawa, K. J. Catalano, M. Delibegovic, J. a Balschi, S. Cinti, B. G. Neel, and B. B. Kahn, *Mol. Cell. Biol.*, 2009, **29**, 4563–73.

50. Y. Okabayashi, S. Tani, T. Fujisawa, M. Koide, H. Hasegawa, T. Nakamura, M. Fujii, and M. Otsuki, *Diabetes Res. Clin. Pract.*, 1990, **9**, 143–8.

51. Y. Nakamura, Y. Tsumura, Y. Tonogai, and T. Shibata, *J. Nutr.*, 1999, **129**, 1214–1222.

52. A. Kumari, V. Kumar, and S. K. Yadav, *PLoS One*, 2012, **7**, e41230.

53. K. D. Arunachalam, L. B. Arun, S. K. Annamalai, and M. Aarrthy, *Int. J. Pharm. Pharm. Sci.*, 2014, **6**, 423–430.

Legends

Fig. 1 The initial colour of $HAuCl_4$ solution (pale yellow) (a) and the final colour of ruby red GA-AuNPs (b).

Fig. 2 The UV-Vis absorption of GA-AuNPs after 1 h and 48 h of GA reaction with $HAuCl_4$. The GA-AuNPs surface plasmon resonance (SPR) appeared at 540 nm.

Fig. 3 The HPLC chromatogram of standard gymnemic acid (a) and GA-AuNPs (b).

Fig. 4 TEM images of GA-AuNPs. It shows the presence of spherical nano particles with sizes ranging from 22-55 nm.

Fig. 5a The size distribution histogram of GA-AuNPs.

Fig. 5b The DLS for zeta potential of GA-AuNPs.

Fig. 6 The XRD spectrum of GA-AuNPs. The characteristic peak for gold (111) was found at $2\Theta = 38.49°$.

Fig. 7 The FT-IR spectrum of plain gymnemic acid (a) and GA-AuNPs (b).

Fig. 8a The *in vitro* stability of GA-AuNPs in different physiological medium. A stable peak appeared for 10% NaCl, 0.5% BSA, 0.2 M Histidine and 0.2 M Cysteine between the range 534-537 nm.

Fig. 8b The *in vitro* stability of GA-AuNPs in phosphate buffer solutions. A stable peak was recorded in phosphate buffer solutions of different pH (1.2, 5, 7.4 & 9) within the range 529-535 nm.

Fig. 9 The cytotoxic activity of GA-AuNPs. Values are means ± SD (n=3 in each group).

Fig. 10 Effect of GA-AuNPs on glucose uptake in cultured 3T3-L1 adipocytes. Values are means ± SD (n=3 in each group). [a] ($p<0.001$) as compared to Control. [b] ($p<0.001$) as compared to Insulin. [c] ($p<0.001$) as compared to Insulin, Pioglitazone, 10 µg mL^{-1} and 30 µg mL^{-1} GA-AuNPS. [d] ns as compared to 30 µg mL^{-1} GA. [e] ($p<0.001$) as compared to Insulin. [f] ns as compared to Pioglitazone.

Scheme I. The proposed modulating action of GA-AuNPs on insulin dependent and independent glucose uptake in 3T3-L1 adipocytes. The GA-AuNPs might act as a suppressor for mitochondrial ATP synthase/PTP-1B. The reduced PTP-1B activity increases the insulin receptor function and GLUT4 translocation, which eventually enhanced the glucose uptake. The GA-AuNPs may be an activator/inducer for AMPK and its pre-signalling molecule LKB1, which induces the translocation of GLUT4 vesicle to the plasma membrane for the insulin independent glucose uptake by the 3T3-L1 adipocytes. GA-AuNPs - Gymnemic acid reduced gold nanoparticles; PTP-1B – Protein tyrosine phosphatase 1B; AMPK – AMP activated protein kinase; LKB-1 – Liver kinase B.

(+) - Inducing action of GA-AuNPs; (-) - Inhibiting action of GA-AuNPs

Figure 1

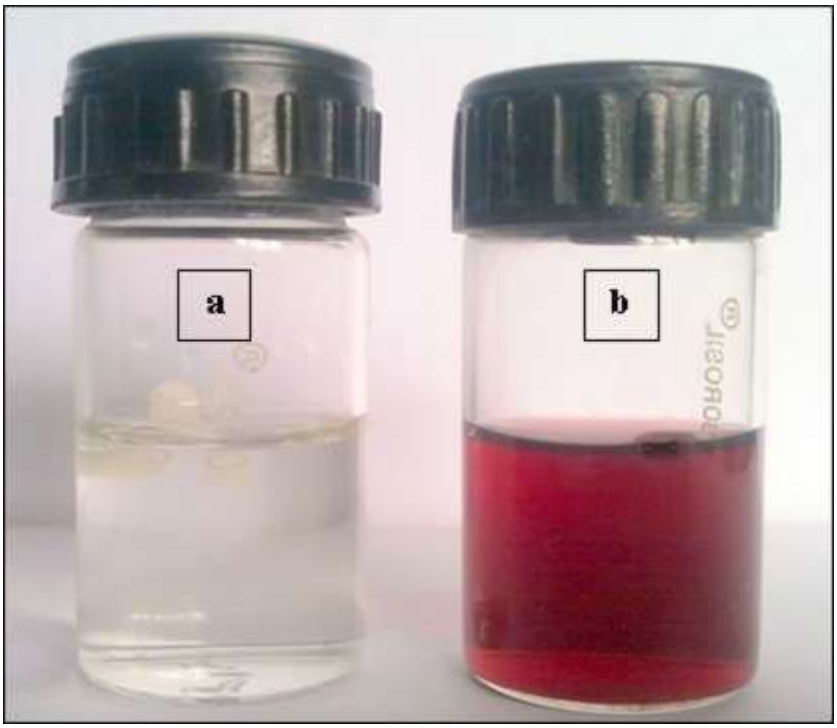

Figure 2

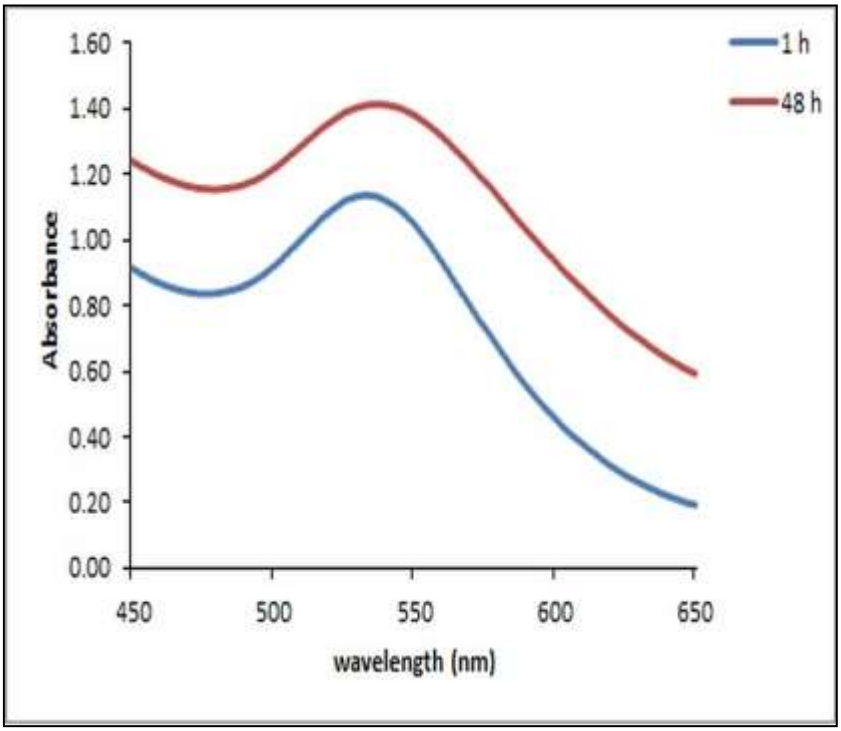

Figure 3a

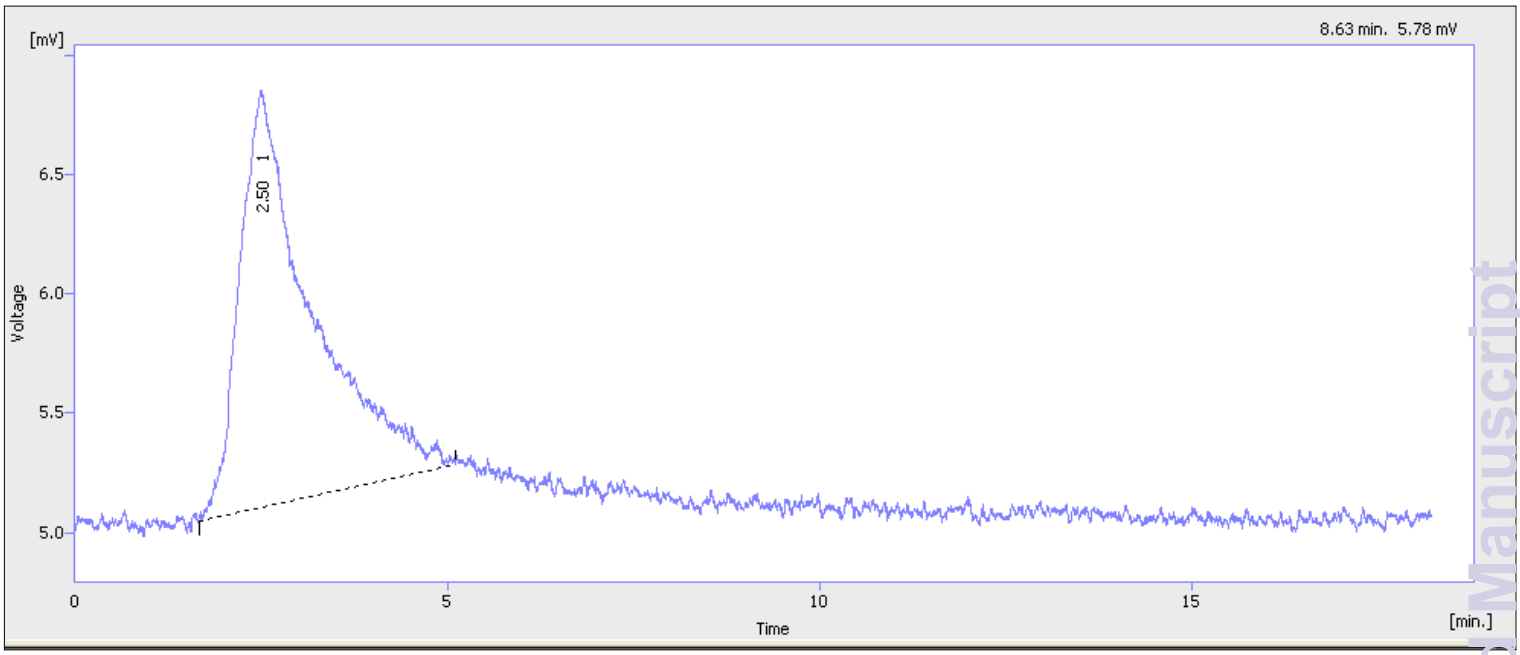

Figure 3b

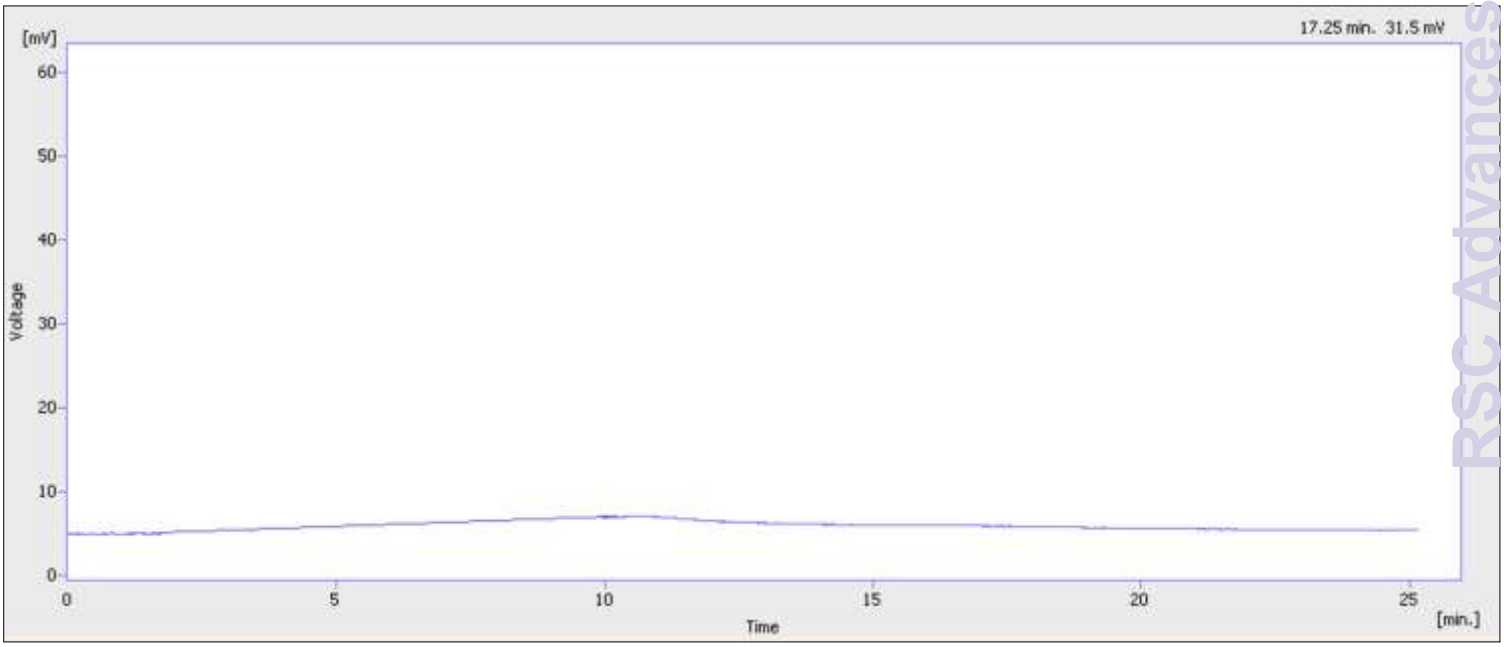

Figure 4

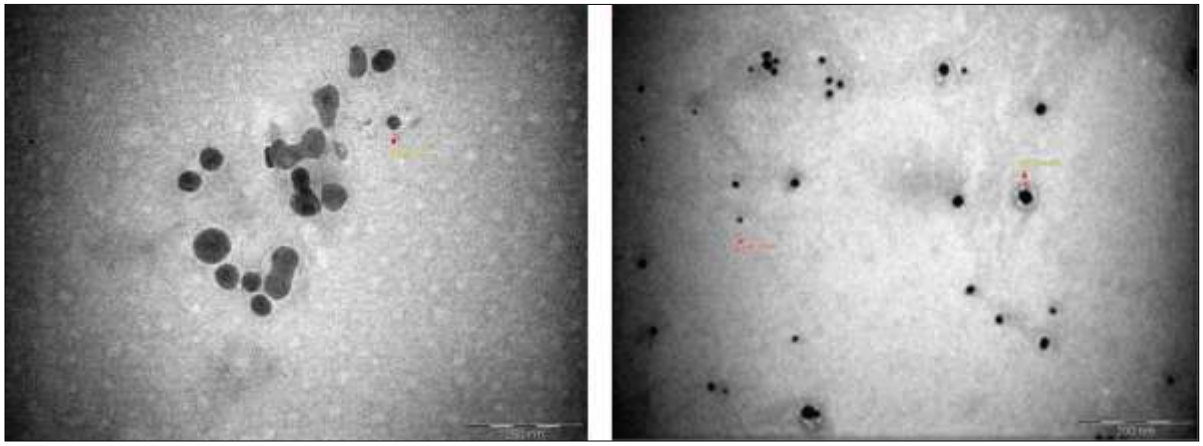

Figure 5a

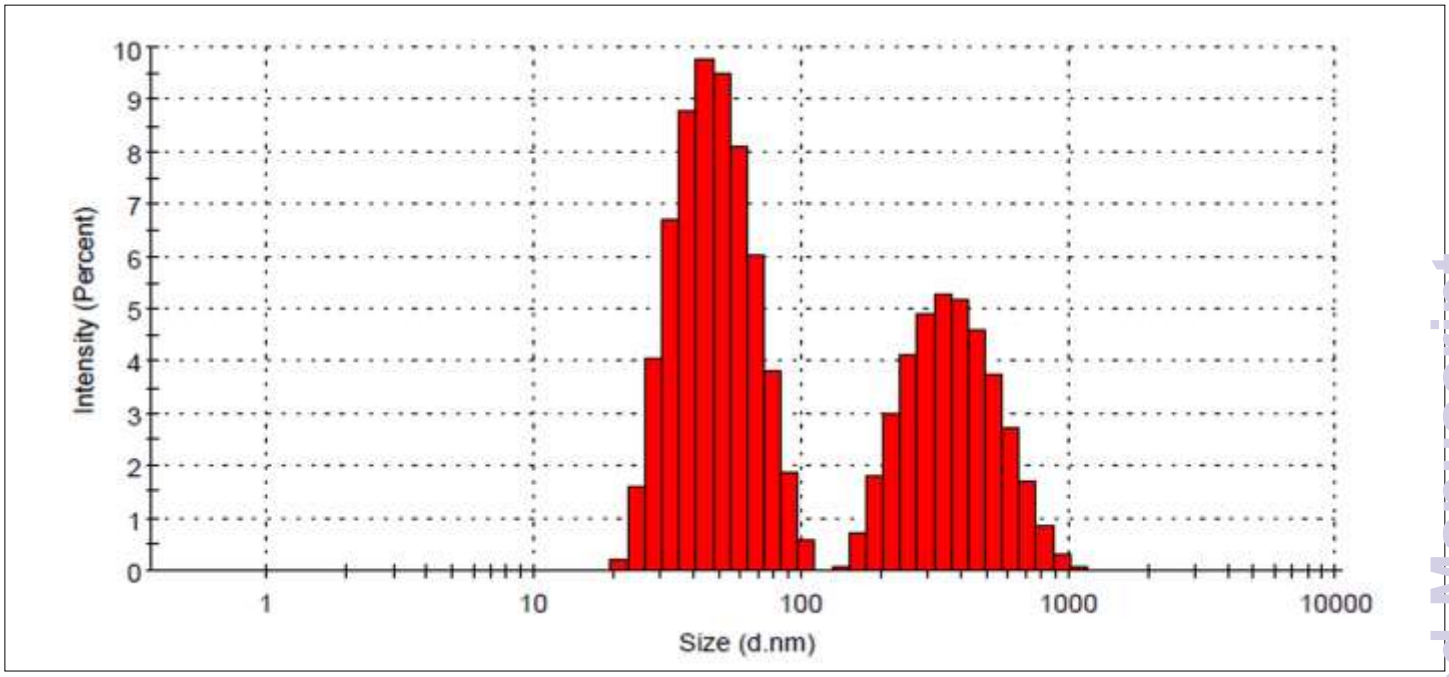

Figure 5b

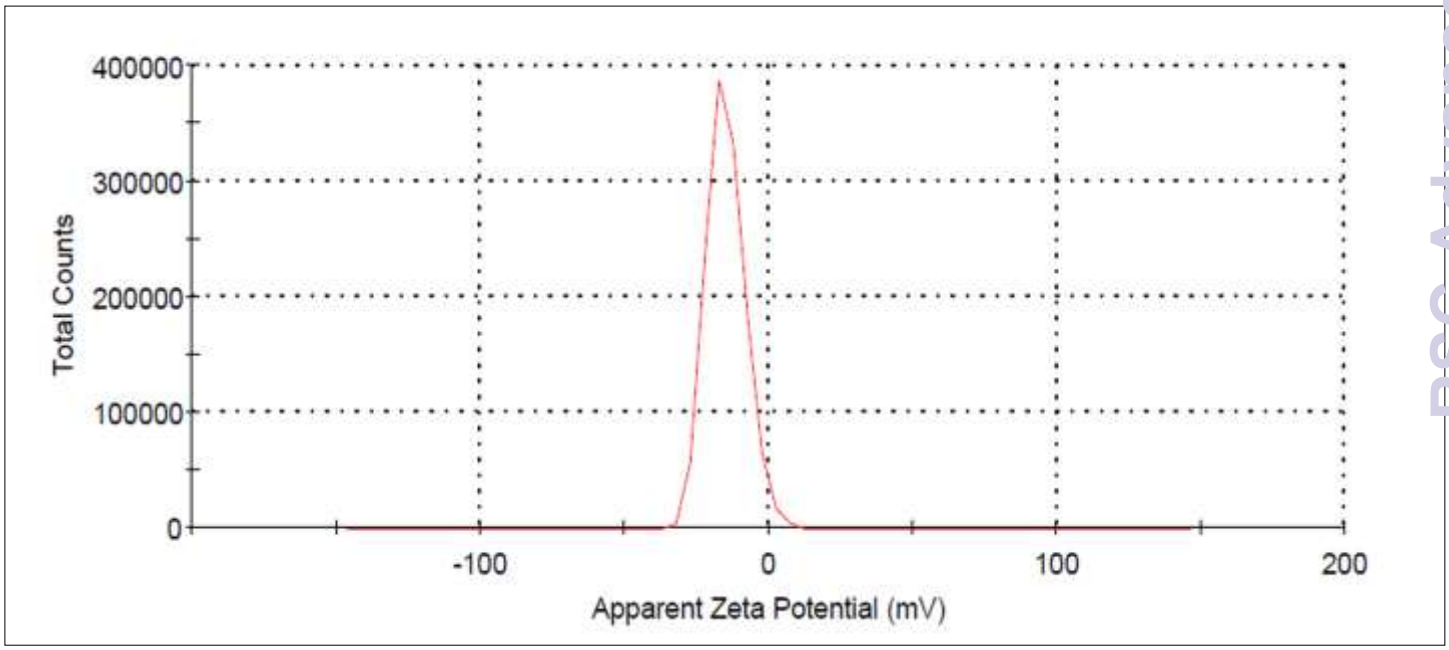

Figure 6

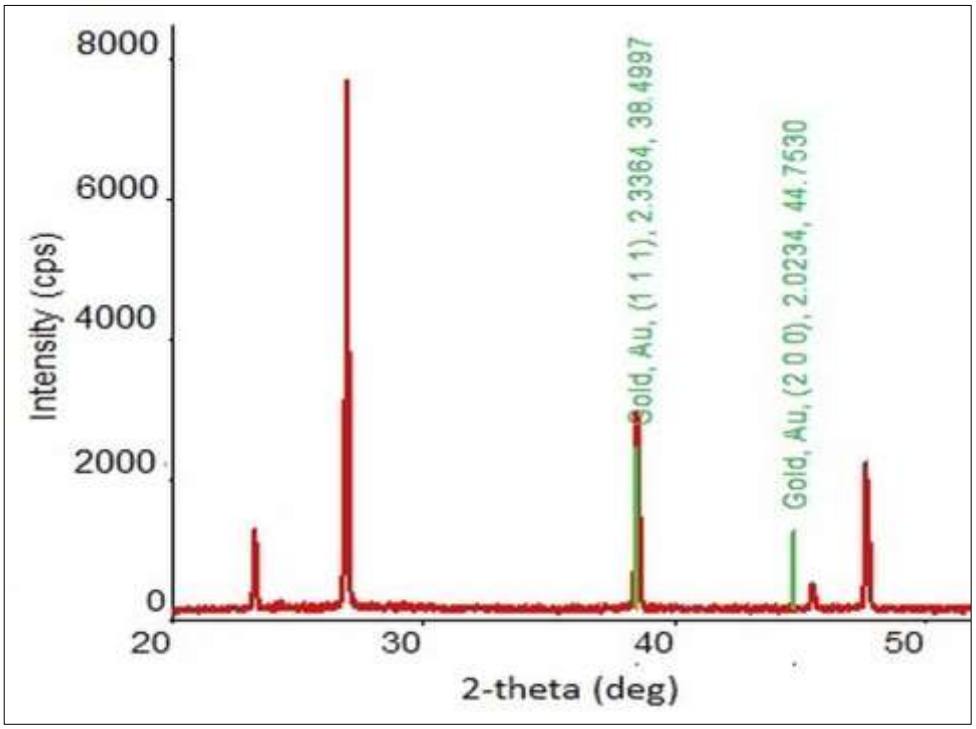

Figure 7

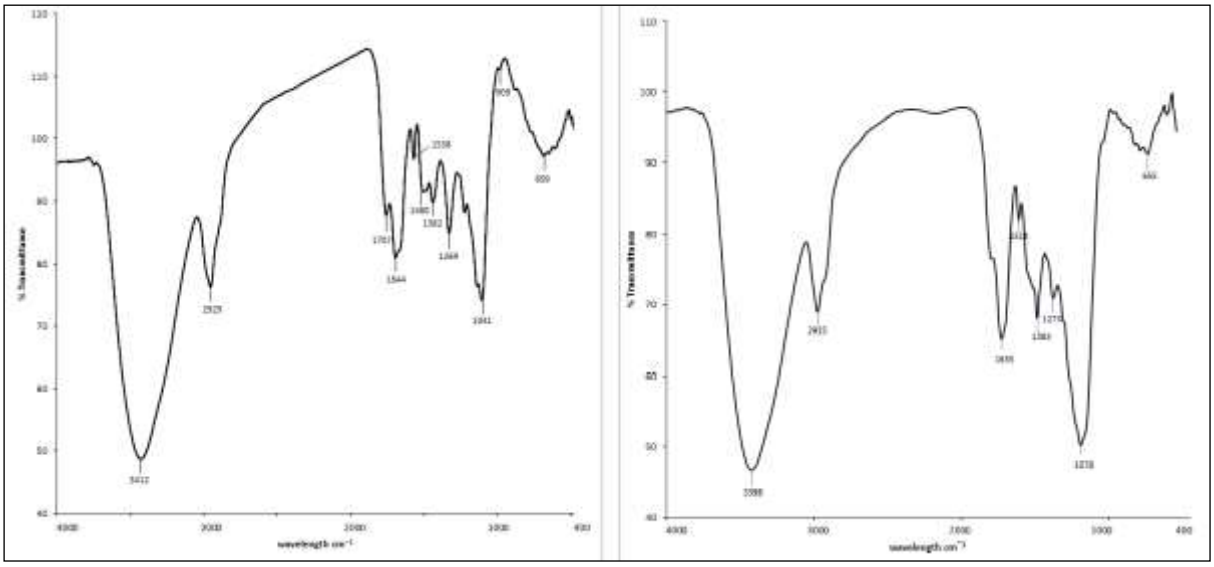

Figure 8a

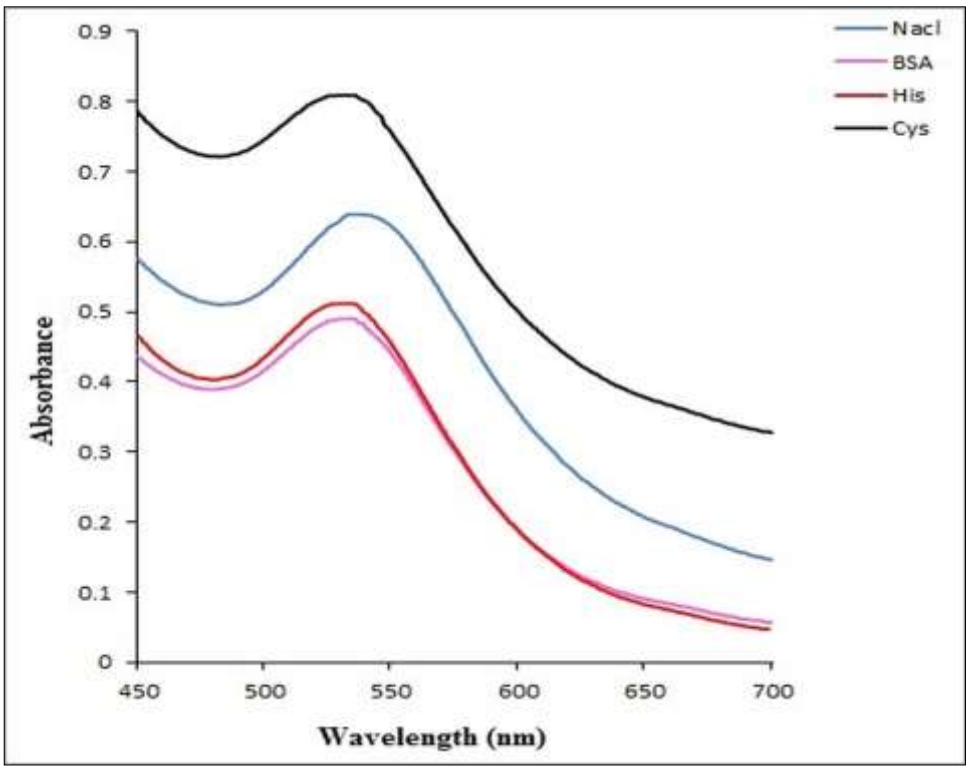

Figure 8b

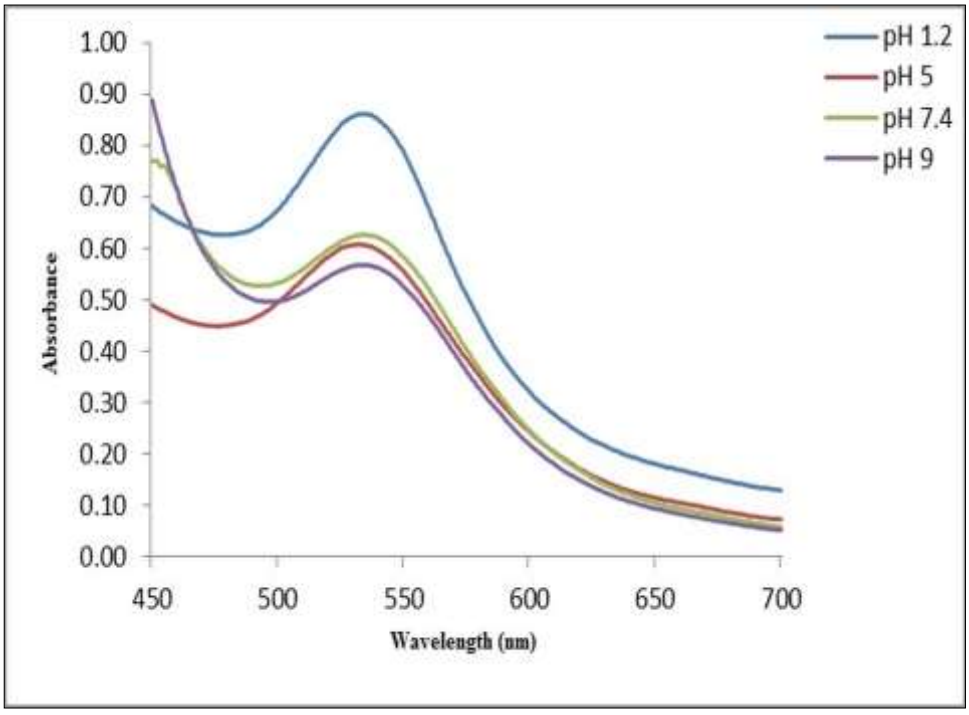

Figure 9

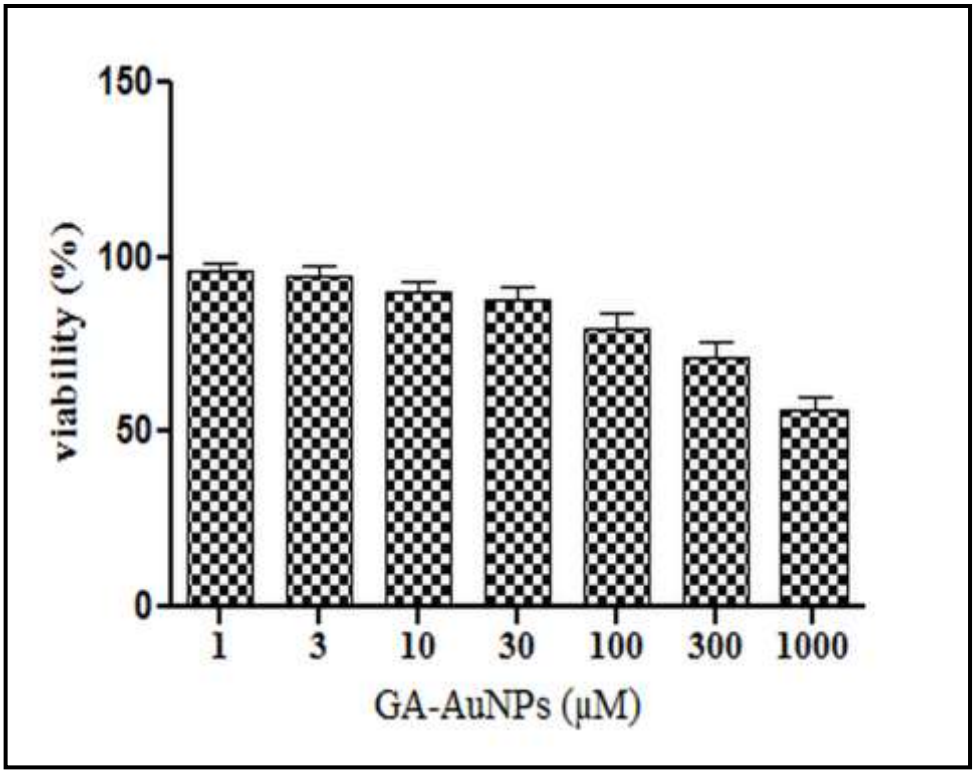

Figure 10

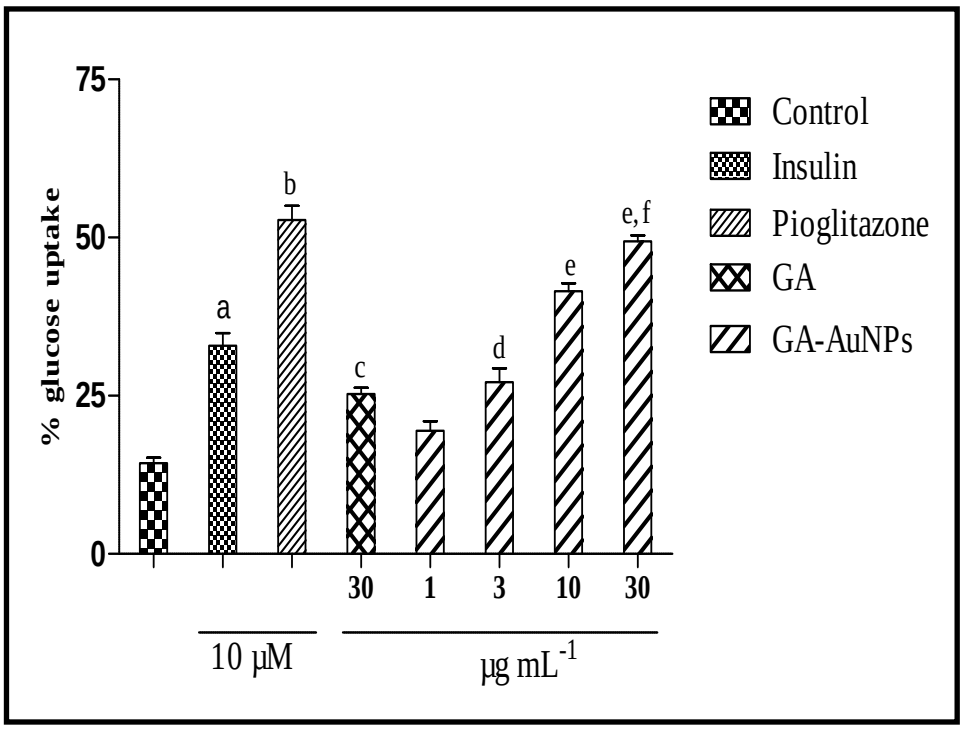

Scheme I

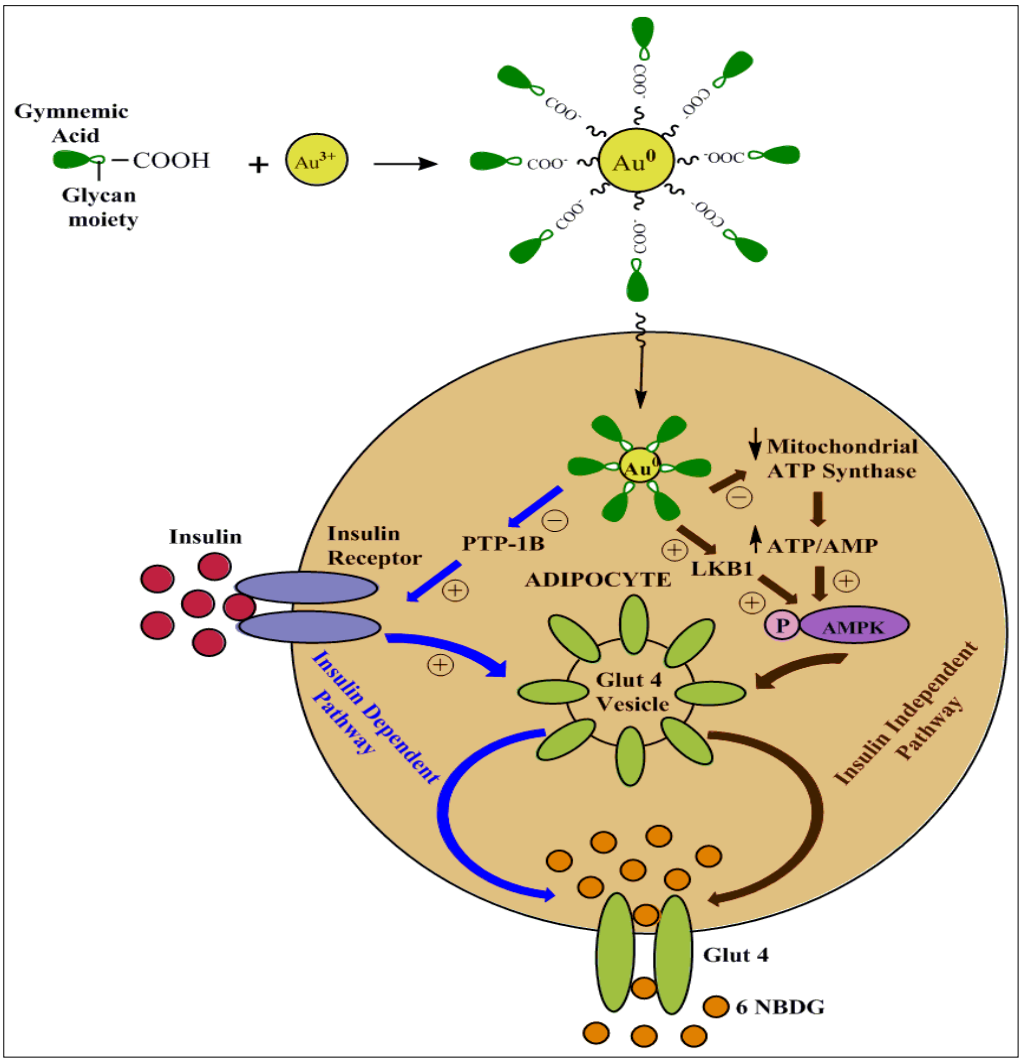

Graphical Abstract